Journal of Power Sources 252 (2014) 51–57

Contents lists available at ScienceDirect

Journal of Power Sources

journal homepage: www.elsevier.com/locate/jpowsour

Non-uniform temperature distribution in Li-ion batteries during discharge – A combined thermal imaging, X-ray micro-tomography and electrochemical impedance approach

James B. Robinson [a], Jawwad A. Darr [b], David S. Eastwood [c], Gareth Hinds [d], Peter D. Lee [c], Paul R. Shearing [a], Oluwadamilola O. Taiwo [a], Dan J.L. Brett [a,*]

[a] Electrochemical Innovation Lab, Department of Chemical Engineering, UCL, London WC1E 7JE, UK
[b] Department of Chemistry, UCL, London WC1H 0AJ, UK
[c] The Manchester X-Ray Imaging Facility, School of Materials, The University of Manchester, Oxford Rd., M13 9PL, UK
[d] National Physical Laboratory, Teddington, Middlesex TW11 0LW, UK

HIGHLIGHTS

- X-ray tomography provides 3D structural map of 18650 battery.
- Heterogeneous temperature distribution above 0.75C.
- Localised heat generation from positive cap containing PTC and safety valve.

GRAPHICAL ABSTRACT

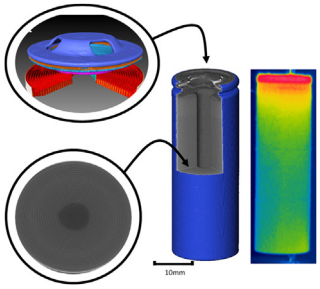

ARTICLE INFO

Article history:
Received 17 July 2013
Received in revised form
28 October 2013
Accepted 1 November 2013
Available online 1 December 2013

Keywords:
Positive temperature coefficient
Thermal imaging
Infrared thermography
Temperature distribution
X-ray tomography
18650 Battery

ABSTRACT

Thermal runaway is a major cause of failure in Li-ion batteries (LIBs), and of particular concern for high energy density transport applications, where safety concerns have hampered commercialisation. A clear understanding of electro-thermal properties and how these relate to structure and operation is vital to improving thermal management of LIBs. Here a combined thermal imaging, X-ray tomography and electrochemical impedance spectroscopy (EIS) approach was applied to commercially available 18650 cells to study their thermal characteristics. Thermal imaging was used to characterise heterogeneous temperature distributions during discharge above 0.75C; the complementary information provided by 3D X-ray tomography was utilised to evaluate the internal structure of the battery and identify the regions causing heating, specifically the components of the battery cap.

1. Introduction

Effective operation of Li-ion battery systems requires careful thermal management in order to ensure stable performance, durable operation and prevent thermal runaway which can lead to catastrophic failure [1]. Poorly designed battery packs can also

* Corresponding author. Tel.: +44(0)20 7679 3310.
E-mail address: d.brett@ucl.ac.uk (D.J.L. Brett).
URL: http://www.ucl.ac.uk/electrochemical-innovation-lab

0378-7753/$ – see front matter © 2013 Elsevier B.V. All rights reserved.
http://dx.doi.org/10.1016/j.jpowsour.2013.11.059

result in significantly reduced volumetric and gravimetric power densities; as such, thermal management strategies are amongst the most important design considerations when developing battery pack systems used in electric vehicles (EVs) and hybrid electric vehicles (HEVs) [2].

The 18650 spiral wound cell is widely used in portable applications, but has also been applied in automotive applications [3]. The design of this cell often incorporates a positive temperature coefficient (PTC) safety device in the battery cap, which demonstrates a large increase in electrical resistance above a certain trigger temperature. When an over-current condition occurs, such as during an electrical short, the high currents cause the heating of the PTC which enters a high-resistance state acting to self-limit the current passed and protect the battery and user from adverse consequences [4]. Although generally an effective safety measure, the incorporation of an additional resistive component acts to increase the internal resistance of the battery (and lower its efficiency) and can generate hazardous temperatures with potential failure leading to fire, causing further damage to the systems which employ such technology, particularly during short circuits [5]. Furthermore, localised temperature variations caused by short circuits or internal defects within individual cells may result in 'hot-spots' within battery packs, leading to thermal runaway which can cause catastrophic failure of whole systems [6]. This has been observed in the grounding of the Boeing 787 'Dreamliner' fleet in 2013 due to faults associated with Li-ion battery packs that included two major battery thermal runaway events in 52,000 flight hours [7] and a fire which occurred in a modified Toyota Prius vehicle due to incorrect electrical contacts within Li-ion battery packs [8]. Given the importance of temperature management in the design of Li-ion systems, a range of electrochemical models have been developed to predict thermal behaviour. These models often make assumptions which neglect non-uniform thermal distributions [9] or have only been validated against a single point temperature measurement, typically made using thermocouple/s on or within the battery/pack [10].

Recent modelling efforts have included attempts to incorporate non-uniform resistance distributions within cells and battery packs [11,12]. These models highlight the importance of thermal management in battery packs and the need for system level experiments. However, the models do not incorporate a PTC element, which will further modify the temperature distribution within packs. In addition, limited experimental validation of the work has been reported, which restricts the use of such models.

Models which fail to take into account the heating effects of 'external' non-electrochemical (ohmic) heat sources, risk eliminating a significant source of heating for a real battery, particularly at high discharge rates. External elements may include a mechanical safety valve, a PTC element or metallic contacts. Yi et al. [13] developed a model which accounts for such resistances in a planar Li-ion cell and attests the importance of characterising these losses.

While much work has gone into producing accurate and robust modelling of Li-ion batteries, experimental validation is required in order to maximise the potential of this area. Discrete thermocouple measurements cannot adequately capture the temporal-spatial dynamics exhibited by batteries and battery packs. The non-invasive nature of thermal imaging, its high temperature resolution and significantly improved spatial resolution represents a much more accurate and representative measurement of the surface temperature of batteries compared to discrete thermocouples.

Wang et al. [14] used infrared thermal imaging on planar Li-ion batteries; however, the work did not investigate the effect of the discharge rate, nor the effect of spatial location on the temperature of the battery. Kim et al. [15,16] reported validation of an electrochemical model using infrared techniques; however, the results were presented for only a single discharge rate.

Schmidt et al. [17] reported a novel electro-thermal impedance spectroscopy (ETIS) technique which can be used to validate electrochemical models by measuring thermal impedance spectra that provide information about the dynamics of heat transfer in the battery structure. While there is great potential in this approach, the use of discrete thermocouples limits spatial resolution and the thermocouples themselves have a thermal response time constant which must be taken into account.

Herein we report the effect of both the discharge rate and time on the spatial temperature distribution of Li-ion batteries (18650 spiral wound) while simultaneously evaluating the electrochemical impedance characteristics of the cell. Additionally, X-ray tomography was conducted to allow the internal structure to be determined and to identify the internal sub-structures which cause non-uniform heating within Li-ion cells. X-ray tomography has proven to be a valuable tool for non-destructive analysis in a wide range of fields. With the increasing sophistication and resolution of tomographic techniques it is now possible to examine batteries over a large range of length scales; from atomic to cell level. The results highlight the importance of robust thermal measurement and give an indication of the spatial and temporal dynamics of temperature change caused by electrical discharge. For the benefit of the battery modelling community, the 3D image data set describing the internal structure of the 18650 cell, including PTC device, is made available for open source usage as supplementary information.

2. Experimental

Experiments were carried out on single 18650 spiral wound lithium nickel manganese cobalt oxide (NMC) Li-ion cells (ICR18650S3, 2200 mAh, LG Chem Ltd., Seoul, South Korea) which have a rated maximum discharge current of 4400 mA (2C). Prior to each test the cell was fully charged to 4.2 V, the maximum rated voltage, first by constant current charging to 4.2 V and a subsequent constant voltage charge at 4.2 V until the current tapered down to 3% of the initial applied current using an electrochemical test station (Maccor 4300, Maccor Inc., Oklahoma, USA) and the manufacturer's recommended charge rate of 0.5C. Although no significant thermal effects were observed during charging at this rate, the cells were disconnected from all electrical contacts for a period of 1 h prior to discharging, to ensure thermal equilibration with ambient temperature. The surface of the battery was coated with a matt black paint to minimise infrared reflections and ensure a uniform emissivity. In order to calculate the emissivity of the coated surface, a purpose-built cavity black-body ($\varepsilon = 0.98$) was used [18] prior to conducting all experiments, in addition to a diffuse reflector which eliminates the effects of environmental reflections.

Thermal imaging was performed using a camera (FLIR SC5000MB, FLIR Systems France, Croissy-Beaubourg, France) which was calibrated for the temperature range in question (15 °C–100 °C). The camera has an extended wavelength detector allowing detection of infrared light within the range 2.5 μm–7 μm. A 27 mm (F/3) lens was used throughout the imaging process, with the images recorded using commercially available software (FLIR Research IR, FLIR Systems, France). The noise-equivalent temperature difference (NETD) of the camera, a measure of the signal-to-noise ratio, was of the order of 19 mK in the range of calibration. The geometry of the experimental setup resulted in a spatial resolution of ~0.1 mm with the images being recorded at a frequency of 1 Hz.

Discharging of the battery was conducted using a potentiostat (IviumStat, Ivium Technologies, Netherlands) at varying C-rates

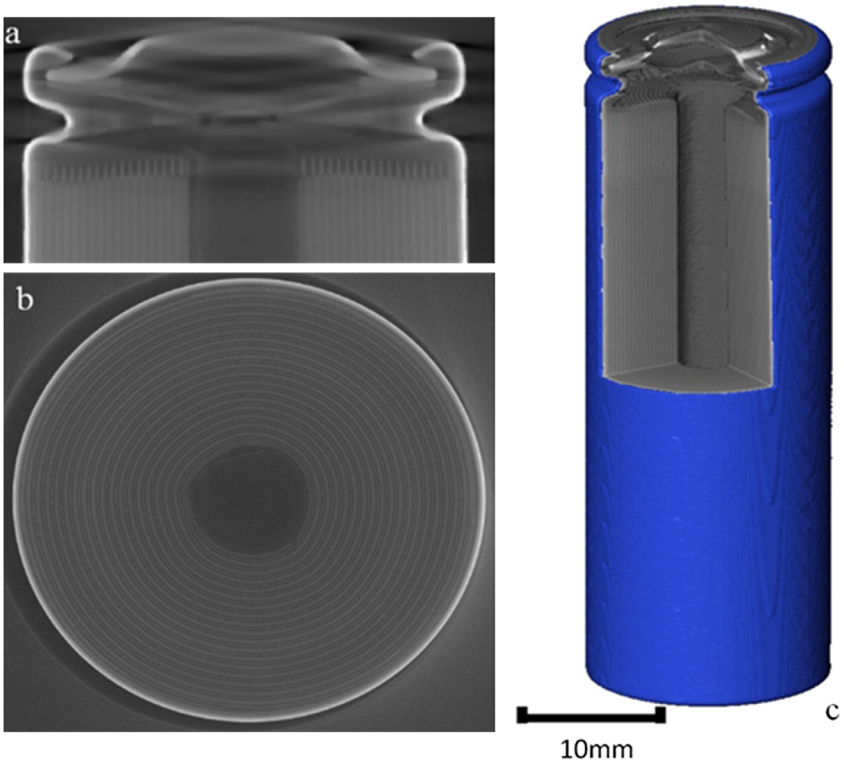

Fig. 1. 3D rendering showing: a) the safety valve assembly in the battery cap, b) a magnified cross section of the battery showing the electrode assembly and hollow centre, and c) a magnified longitudinal slice of the battery.

within the safe discharge regime, according to the cell manufacturer. Potentiostatic Electrochemical Impedance Spectroscopy (EIS) was conducted from 10 kHz to 1 Hz using a 15 mV AC sinusoidal perturbation at the open circuit voltage (OCV).

An environmental chamber was used to assess the effect of temperature on the electrochemical impedance response and to determine the onset of increased resistance due to thermal activation of the PTC element. The chamber consisted of a PID controlled electronic heater which enabled the temperature within the enclosure to be controlled to ± 1 °C of the desired set point. During the experiments the chamber was allowed to reach thermal equilibrium for a period of no less than 10 min prior to experiments to minimise the inherent PID control fluctuations in temperature.

In order to ensure the battery was without any structural defects and to determine the assembly and location of internal components, X-ray tomography was conducted at the Manchester X-Ray Imaging Facility at Harwell. Tomography scans of the positive terminal region and of the full battery were obtained, and subsequent 3D analysis of the reconstructed image data was performed using Avizo software (FEI Company, Oregon, USA). X-ray microtomography scans were performed on the battery using a Phoenix v|tome|x system (Phoenix X-ray, GE Measurement and Control, Germany). The battery was rotated 360° about its long axis whilst 1000 projections were captured with the nanofocus tube operating at 100 kV and 270 μA. The sample and detector were positioned in projection magnification providing an effective pixel size of 8.94 μm for the high resolution imaging.

3. Results and discussion

3.1. X-ray tomography

In order to associate external measures of temperature with internal heat generation sources, an understanding of the internal

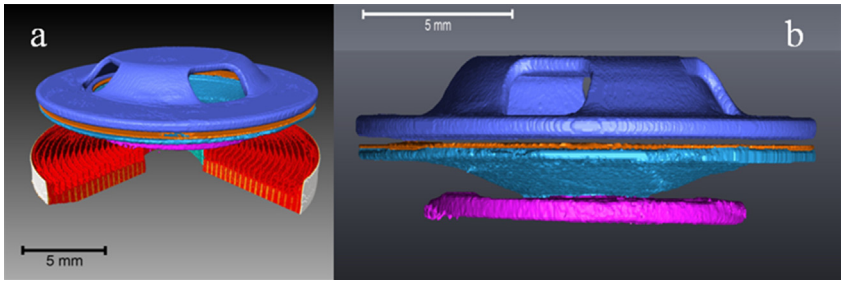

Fig. 2. 3D reconstruction showing: a) auxiliary view of the safety valve area highlighting the positive electrode contactor (purple), PTC element (orange) and safety valve (turquoise); b) orthographic view of the positive terminal area. (For interpretation of the references to color in this figure legend, the reader is referred to the web version of this article.)

structure of the battery is desirable. While the 18650 (18 mm diameter, 65 mm high) battery is a widely used standard, the internal configuration can vary between manufacturer and internal defects can arise due to manufacturing tolerances and material processing variability. Disassembly of a battery is both a hazardous and destructive process. X-ray tomography has been shown to be a powerful, non-destructive tool for the characterisation of the structure of electrodes, single cells and devices [19–21]. Fig. 1 shows a 3D rendering of the tomographic data set for the 18650 cell. The spirally wound internal structure of the cell, separator material and hollow central section, is clearly visible in Fig. 1(b).

No macro-structural defects were observed within the cell, which could give rise to undesirable sources of heat. The X-ray micro-tomography also enabled a reconstruction of the battery cap architecture (Fig. 2), including the valve, PTC and positive electrode terminal.

The tomographic reconstructions show the tightly packed nature of the positive terminal area. The entire battery cap (terminal and safety componentry) is ~5 mm in height.

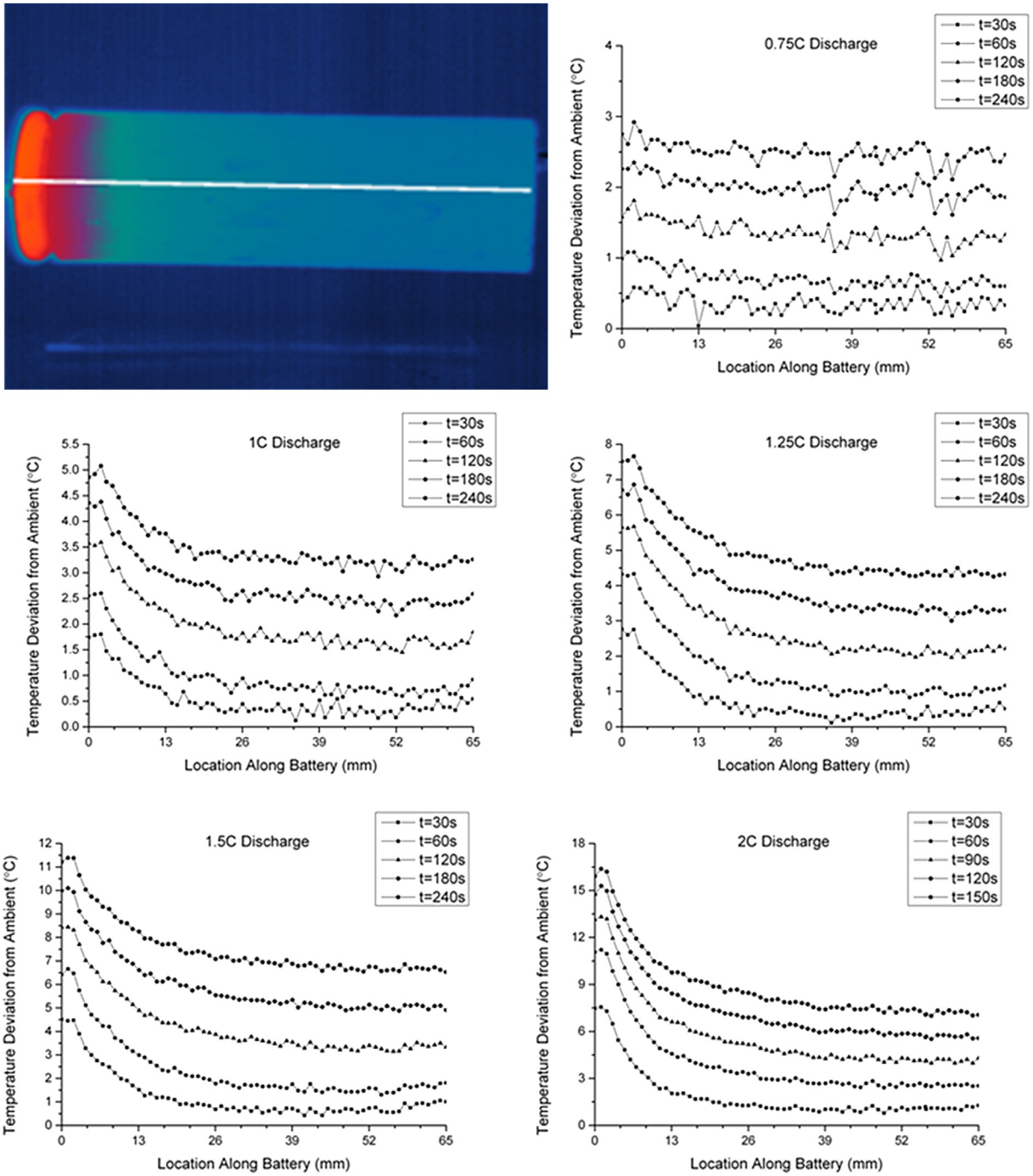

Fig. 3. Axial line of measurement and temperature deviation distributions as a function of location along battery and time (in seconds) during 0.75C–2C discharge.

3.2. Thermal imaging

Infrared imaging was conducted while the battery was discharged at a range of discharge rates, ranging from C/10 to 2C. Average battery temperatures rose with time during discharge as a result of heat generation associated with reaction and Joule heating, with significant spatial variations observed along the length of the battery. The local temperature along the central-line of the battery was captured, as indicated in the inset in Fig. 3, with local temperature deviations from ambient as a function of time and discharge rate plotted in Fig. 3.

Fig. 3 shows the increasing heterogeneity of temperature distribution along the longitudinal axis of the cell with increasing discharge rate. No significant temperature heterogeneity was observed for discharge up to 0.75C. At discharge rates higher than 1C an area of increased temperature is identifiable 0 mm–4 mm from the positive terminal of the battery. This area corresponds to the battery cap, as identified by the X-ray tomography. The temperature at the surface of the battery cap is seen to be larger than that along the body of the battery purely due to the discharging process; this implied a higher rate of heat generation at the positive terminal than in the bulk of the battery itself. From the micro-tomograms it was deduced that this increased rate of heat generation can be attributed to the battery terminal area due to its non-uniform nature and multi-component construction.

By comparing the temperature rise at both terminals it can be concluded that the contact resistance with the external current collector did not contribute greatly to the thermal gradient. This is particularly evident for the 1C–2C discharge rates, during which a significant temperature gradient was observed close to the positive terminal but with no similar gradient appearing at the negative terminal. This implies that the battery cap provides a significantly higher resistance to current flow; resulting in the increased heat generation and corresponding temperature rise. It has been reported that safety valves used within Li-ion batteries are either composed of an aluminium or aluminium/polymer structure [22], the bulk material of which will not add significantly to the resistance of the cell due to the high electrical conductivity. It is therefore proposed that the contact resistance between components in the cap and the PTC element provides sufficient resistance to cause the thermal gradients observed.

As PTC elements are designed to be activated (increase in electrical resistance) at elevated temperatures, it is important to consider not only surface temperature but also internal temperature, which may vary considerably from that measured at the surface [23].

It is evident from Fig. 3 that, for discharge rates of 1C and above, increasing current leads to a higher temperature gradient close to the positive terminal of the battery. However, the temperature profile itself does not change appreciably with time at each discharge current, with a relatively uniform increase in temperature observed along the length of the cell.

The temperature heterogeneity highlighted above is particularly relevant to the positioning of thermocouples in battery packs. If the thermocouple is located towards the negative terminal of a battery the error in measuring the peak temperature of the cell may be particularly large; something which when incorporated into a battery pack may have severe consequences. The fact that cells are typically uniformly aligned within battery packs will tend to create an area of high heat output at the positive terminal current collector.

In addition to examining the axial temperature distribution, the 'surface hoop circle' distribution within cylindrical Li-ion cells was also investigated. It can be seen in Fig. 4 that provided the current collectors are positioned in the centre of the electrode terminal, there is no significant thermal variation around the cell housing.

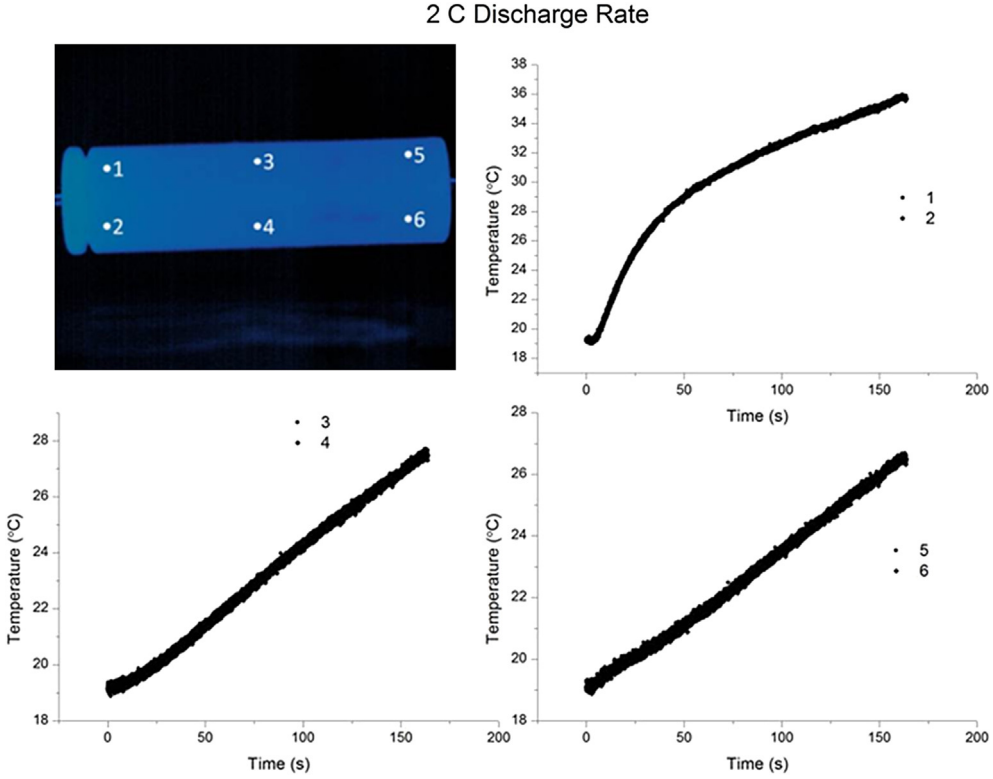

Fig. 4. Transient temperature response at different locations along the axis of the battery (30 mm approx. between each point axially, 5 mm approx. between each point along the surface hoop circle) at a 2C discharge rate.

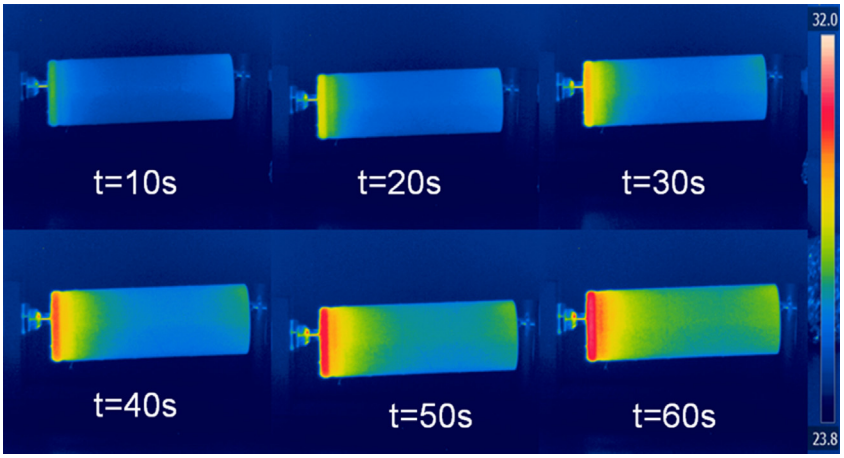

Fig. 5. Effect of acentric current collection from a pin current collector on the positive (left hand side) and negative (right hand side) electrode during a discharge at a rate of 2C during a 60 s period.

However, poor electrical contact can lead to significant heterogeneity in the radial temperature distribution and additional heating at the electrode terminals. For example, Fig. 5 shows the case of an acentric current collector pin at the negative electrode terminal the poor mechanical coupling (low clamping force) led to localised Joule heating and the acentric connection led to heating from the point of contact, causing a radially non-uniform heat distribution. This effect is also observed at the positive terminal; however, due to the magnitude of the heating in this region the effect is less pronounced than at the negative terminal. These effects manifest themselves in non-uniform temperature gradients across the battery surface and further add to the limitations of not including non-electrochemical elements when modelling battery temperatures.

3.3. Electrochemical impedance spectroscopy

Electrochemical impedance spectroscopy was conducted on the cell at various temperatures at OCV in order to decouple the thermal effects on the various loss mechanisms in the battery.

The typical EIS response of Li-ion cells is composed of a bulk ohmic resistance coupled with two overlapping RC arcs corresponding to solid-state resistance and capacitance at high frequencies and charge transfer resistance and the associated double-layer capacitance at intermediate frequencies [24]. In addition, at low frequency a Warburg element accounts for the diffusional limitation associated with the mass transfer of lithium ions between the electrodes and the electrolyte.

Fig. 6 shows the electrochemical impedance response in complex plane (Nyquist plot) form at OCV as a function of temperature. It was not possible to resolve two arcs for all temperatures, either because one of the RC couples was much smaller than the other and/or the time constant for each process was not significantly different; however, an indication of a secondary arc is visible at 20 Hz at a temperature of 23 °C, indicating the presence of two independent processes. A Warburg impedance feature at low frequency (<10 Hz in all cases) is clearly evident. Nagasubramanian has demonstrated the effects of temperature on 18650 Li-ion cells, showing a reduction in the overall electrochemical impedance with increasing temperature and an approximately stable ohmic resistance, given by the high frequency intercept [25]. In agreement

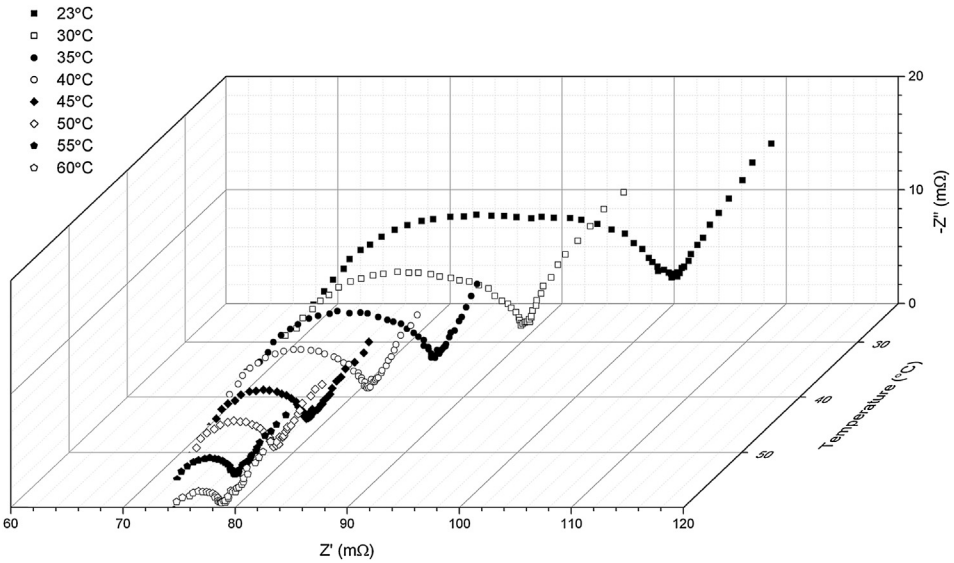

Fig. 6. Effect of temperature on the EIS sweeps at OCV conducted within an environmental chamber over the temperature range of 23–60 °C.

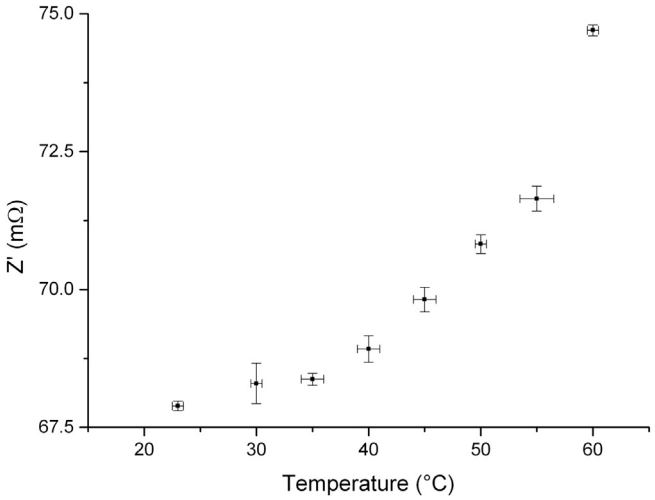

Fig. 7. Effect of temperature upon the location of the high frequency intercept (purely ohmic resistance) showing the standard deviation of the EIS measurements and the range of temperature fluctuation throughout the duration of the measurement.

with this study, a reduction in the primary arc resistance was observed with increasing temperature up to 60 °C.

The purely ohmic component (determined from the high frequency intercept with the real axis) as a function of temperature is shown in Fig. 7. The observed effect of temperature on the ohmic resistance within the temperature range 20–40 °C is in agreement with the results reported by Nagasubramanian [25]; however, above 40 °C an increase in ohmic resistance is observed which is attributable to an increase in resistivity of the metallic elements within the cell.

The effect of temperature upon the resistance of PTC elements has been reported at higher temperatures in a $LiFePO_4$ cell by Zhong et al. [26]. By comparing the relative changes in magnitude of resistance it is clear that the PTC has not been activated during the experiments conducted in this study. The EIS data shown here imply that the PTC effect does not contribute to the asymmetric heating of the cell due to increased resistance over the relevant temperature range in this study; rather, it is the presence of the PTC and safety valve at the positive terminal which drive the heating by a non-uniform distribution of ohmic resistance within the cell.

4. Conclusions

Heterogeneous temperature distribution across the length of a single 18650 Li-ion cell has been observed for discharge rates above 0.75C, within the standard operating window of the cell. External electrical contact resistances at both terminals can contribute to this at higher current densities; however, the most significant heating effect is observed within the cell at the positive terminal. The high resolution thermal images show that discrete thermocouples cannot fully capture the thermal profile and the location of placement is important for safety purposes and should be sited close to the positive cap of the cell.

X-ray micro-tomography provides a clear picture of the internal structure of the battery and shows that the source of the heating corresponds to the PTC and safety valve assembly. EIS as a function of whole-cell temperature shows that this particular PTC is not significantly activated at temperatures up to 60 °C. Given that the high discharge rates studied (up to 2C) did not lead to cell temperatures anywhere as high as this, activation of the PTC is not expected to occur. Rather, the heating effect in the positive cap is attributed to the materials and internal contact resistances between the battery roll, PTC and safety valve.

Models must consider spatially allocating the ohmic resistances within cells in order to give a truly accurate representation of both the thermal and electrochemical effects of the system. In addition, the non-uniform materials of the cell must be accounted for in order to capture the dynamics of battery discharge which have been shown to significantly deviate from a 'quasi' steady-state or uniform thermal distribution assumption often made when producing electro-thermal models. Finite element models that consider the internal structure of the battery must consider the features in the cap and structure of the 'jelly roll' and casing. To this end, data is provided with this paper to describe the structure, based on X-ray tomography, for this common battery architecture.

Acknowledgements

The authors would like to acknowledge the EPSRC funding for supporting the work of Robinson and Brett (EP/J001007/1); the STFC for supporting Shearing and Brett (ST/K00171X/1); the Office of Naval Research and Royal Academy of Engineering for supporting Shearing.

References

[1] M. Winter, R.J. Brodd, Chem. Rev. 104 (2004) 4245–4270.
[2] T.M. Bandhauer, S. Garimella, T.F. Fuller, J. Electrochem. Soc. 158 (2011) R1–R25.
[3] X. Qiu, X. Zheng, J. An, W. Zhu, Method for producing assembled battery and assembled battery. US 2012/0114995.
[4] G. Venugopal, J. Power Sources 101 (2001) 231–237.
[5] A.A. Pesaran, G.H. Kim, K. Smith, Lithium Mobile Power: Advances in Lithium Battery Technologies for Mobile Applications, third ed., Knowledge Press, Boston, 2008.
[6] C.Y. Jhu, Y.W. Yang, C.Y. Wen, C.M. Shu, Appl. Energy 100 (2012) 127–131.
[7] NTSB, Interim Factual Report DCA13IA037, Boston, 2013.
[8] G.P. Beauregard, Report of Investigation: Hybrids Plus Plug in Hybrid Electric Vehicle, U.S. Department of Energy, Idaho National Laboratory, 2008.
[9] Y. Ji, Y. Zhang, C.Y. Wang, J. Electrochem. Soc. 160 (2013) A636–A649.
[10] Y. Ye, Y. Shi, N. Cai, J. Lee, X. He, J. Power Sources 199 (2012) 227–238.
[11] B. Wu, V. Yufit, M. Marinescu, G.J. Offer, R.F. Martinez-Botas, N.P. Brandon, J. Power Sources 243 (2013) 544–554.
[12] F. Jiang, P. Peng, Y. Sun, J. Power Sources 243 (2013) 181–194.
[13] J. Yi, U.S. Kim, C.B. Shin, T. Han, S. Park, J. Electrochem. Soc. 160 (2013) A437–A443.
[14] Z.J. Wang, Z.Q. Li, Q. Liu, SPIE Proceedings 8913 (2011).
[15] U.S. Kim, C.B. Shin, C.S. Kim, J. Power Sources 180 (2008) 909–916.
[16] U.S. Kim, C.B. Shin, C.S. Kim, J. Power Sources 189 (2009) 841–846.
[17] J.P. Schmidt, D. Manka, D. Klotz, E. Ivers-Tiffée, J. Power Sources 196 (2011) 8140–8146.
[18] M. Vollmer, K.P. Mollmann, Infrared Thermal Imaging, Wiley-VCH, Weinheim, 2010.
[19] P.R. Shearing, L.E. Howard, P.S. Jorgensen, N.P. Brandon, S.J. Harris, Electrochem. Commun. 12 (2010) 374–377.
[20] V. Yufit, P. Shearing, R.W. Hamilton, P.D. Lee, M. Wu, N.P. Brandon, Electrochem. Commun. 13 (2011) 608–610.
[21] P.R. Shearing, N.P. Brandon, J. Gelb, R. Bradley, P.J. Withers, A.J. Marquis, S. Cooper, S.J. Harris, J. Electrochem. Soc. 159 (2012) A1023–A1027.
[22] P.G. Balakrishnan, R. Ramesh, T. Prem Kumar, J. Power Sources 156 (2006) 401–414.
[23] C. Forgez, D.V. Do, G. Friedrich, M. Morcrette, C. Delacourt, J. Power Sources 195 (2010) 2961–2968.
[24] S.S. Zhang, K. Xu, T.R. Jow, Electrochim. Acta 49 (2007) 1057–1061.
[25] G. Nagasubramanian, J. Power Sources 87 (2000) 226–229.
[26] H. Zhong, C. Kong, H. Zhan, C. Zhan, Y. Zhou, J. Power Sources 216 (2012) 273–280.